



This is a repository copy of *Optimisation and analysis of a heat pipe assisted low-energy passive cooling system*.

White Rose Research Online URL for this paper:
<http://eprints.whiterose.ac.uk/112673/>

Version: Accepted Version

Article:

Chaudhry, H.N., Calautit, J.K. and Hughes, B.R. (2017) Optimisation and analysis of a heat pipe assisted low-energy passive cooling system. *Energy and Buildings*. ISSN 0378-7788

<https://doi.org/10.1016/j.enbuild.2017.02.002>

Reuse

This article is distributed under the terms of the Creative Commons Attribution-NonCommercial-NoDerivs (CC BY-NC-ND) licence. This licence only allows you to download this work and share it with others as long as you credit the authors, but you can't change the article in any way or use it commercially. More information and the full terms of the licence here: <https://creativecommons.org/licenses/>

Takedown

If you consider content in White Rose Research Online to be in breach of UK law, please notify us by emailing eprints@whiterose.ac.uk including the URL of the record and the reason for the withdrawal request.



eprints@whiterose.ac.uk
<https://eprints.whiterose.ac.uk/>

Optimisation and analysis of a heat pipe assisted low-energy passive cooling system

Dr. Hassam Nasarullah Chaudhry¹

School of Energy, Geoscience, Infrastructure and Society, Heriot-Watt University, PO Box 294
345, Dubai, United Arab Emirates

Contact: +971 (0) 4 435 8775, Email: H.N.Chaudhry@hw.ac.uk

Dr. John Kaiser Calautit

Department of Mechanical Engineering, University of Sheffield, S10 2TN, UK

Email: j.calautit@sheffield.ac.uk

Dr. Ben Richard Hughes

Department of Mechanical Engineering, University of Sheffield, S10 2TN, UK

Email: ben.hughes@sheffield.ac.uk

Abstract

Passive cooling using windcatchers have been utilised in the past by several Middle East countries to capture wind and provide indoor ventilation and comfort without using energy. Recently, researchers have attempted to improve the cooling performance of windcatchers by incorporating heat pipes. The present work encompasses existing research by optimising the arrangement of heat pipes in natural ventilation airstreams using numerical and experimental tools. The airflow and temperature profiles were numerically predicted using Computational Fluid Dynamics (CFD), the findings of which were quantitatively validated using wind tunnel experimentation. Using a source temperature of 314K or 41°C and an inlet velocity of 2.3m/s, the streamwise distance-to-pipe diameter ratio was varied from 1.0 to 2.0 and the emergent cooling capacities were established to comprehend the optimum arrangement. The results of this investigation indicated that the heat pipes operate at their maximum efficiency when the streamwise distance is identical to the diameter of the pipe as this formation allows the incoming airstream to achieve the maximum contact time with the surface of the pipes. In addition, the findings showed that any increase in streamwise spacing leads to the formation of a second bell curve representing an increase in air velocity which simultaneously reduces the contact time between the airstream and the heat pipes, decreasing its effectiveness. The study quantified that the optimum streamwise distance was 20mm at which the Sd/D (streamwise distance-to-pipe diameter) ratio was 1.0. The thermal cooling capacity was subsequently found to decrease by 10.7% from 768W to 686W when the streamwise distance was increased to 40mm (Sd/D ratio of 2.0). The technology presented here is subject to an international patent application (PCT/GB2014/052263).

Keywords: Cooling capacity; heat pipe; streamwise; temperature; wind tunnel

Nomenclature:

¹Corresponding author

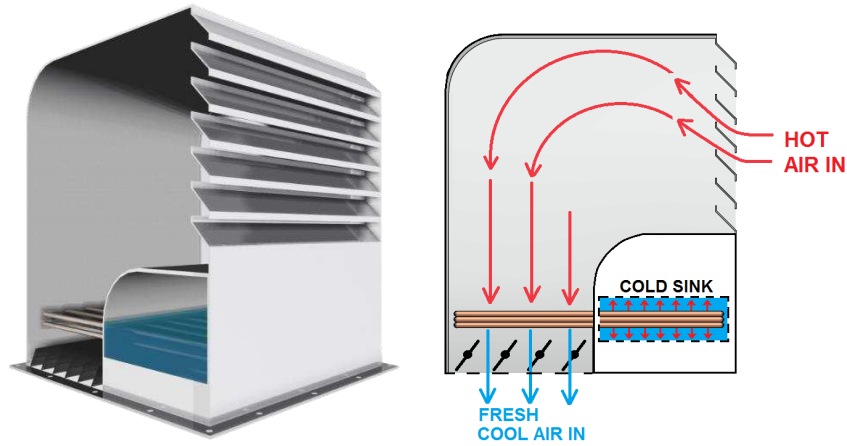
37	A	Cross sectional area (m^2)
38	ρ	Density of liquid (kg/m^3)
39	ε	Effectiveness of heat exchanger
40	g	Gravitational acceleration (m/s^2)
41	q_{actual}	Heat transfer, actual (W)
42	q_{max}	Heat transfer, ideal (W)
43	q_e	Heat transfer rate to evaporator (W)
44	h_{fg}	Specific enthalpy (J/kg)
45	c_p	Specific heat capacity of liquid (J/kgK)
46	ΔT	Temperature difference (K)
47	$T_{c,inlet}$	Temperature at inlet to condenser (K)
48	$T_{e,inlet}$	Temperature at inlet to evaporator (K)
49	$T_{e,outlet}$	Temperature at outlet from evaporator (K)
50	U	Velocity (m/s)

51 **1. INTRODUCTION**

52 The way in which heat pipes are arranged plays an imperative role on the overall effectiveness of the
53 technology, especially when employed as a passive cooling component in natural ventilation systems.
54 Although a lot of advancements have been made in the field of natural ventilation, they have their
55 own limitations in terms of delivering adequate indoor cooling temperatures largely due to external
56 climatic variations in hot countries. Therefore, the optimisation of passive cooling using energy-
57 efficient heat pipes is of significant interest in the ventilation sector. By incorporating the zero-energy
58 working principles of heat pipes to provide the cooling duty, natural ventilation systems can become
59 an effective and sustainable alternative in keeping the internal environment comfortable [1-3].

60 Existing research has indicated the integration of heat pipes into a passive cooling windcatcher to
61 improve its thermal performance [4]. Wind catchers are traditional natural ventilation systems based
62 on the design of traditional architecture, intended to provide ventilation by manipulating pressure
63 differentials around buildings induced by wind movement and temperature difference. Figure 1
64 displays the cooling operation of a windcatcher with heat pipes inside its channel. The system
65 provides natural ventilation inside a building by capturing warm/hot outdoor air and passing it
66 through the evaporator side of heat pipes which absorbs the thermal energy from the passing airflow
67 and transfer it to a parallel cold sink (condenser). Heat pipes transfer only sensible energy from one
68 airstream to another. Heat pipes do not have moving parts, and failure of the entire unit is infrequent
69 due to minimal risk of corrosion and wear. Space efficiency is another typical characteristic of heat
70 pipes as they can be manufactured in various dimensions depending on the configuration of the
71 energy system. Heat pipes are energy-efficient passive devices and do not consume fossil fuels and
72 other environmentally hazardous resources for carrying out its operation, thereby making itself
73 extremely suitable for use in natural ventilation air streams. There are various heat pipe systems
74 currently available which are applicable to operating temperatures associated with building energy
75 applications [4].

76



77

78

Figure 1 A passive cooling windcatcher with heat pipes to optimise cooling performance

79

80

81

82

83

84

85

A wide range of studies have been carried out in order to comprehend the thermal behaviour of heat pipes when arranged in a staggered or an inline grid. Generally, staggered arrangements have been found to be more effective than the inline method [5-8]. However, the research on evaluation and optimisation of the cooling capacity of heat pipes in response to varying streamwise configurations are limited in particular its applications in windcatchers. This work therefore investigated the sensible heat transfer and effectiveness of heat pipes in ventilation airstreams by investigating varying streamwise arrangements.

86

2. PREVIOUS RELATED WORK

87

88

89

90

91

92

93

94

95

96

97

Yodrak et al., [9] carried out work on analysing the thermal performance of heat pipes when arranged in both staggered and inline grids. The heat pipe comprised of an evaporator and condenser length of 0.15m along with an adiabatic section of 0.05m. Water was used as the internal working fluid and the internal diameter of the steel heat pipe tube was 0.02m. The arrangement comprised of a total of 8 rows with 6 tubes in each row. Measurements were recorded at the inlet and outlet of the evaporator and condenser section when a steady-state was achieved wherein the temperatures normalised. K-type thermocouples were used as instrumentation for temperature measurement. The mass flow rate of the incoming fluid to the evaporator section was 0.0098 kg/sec. The results of the study established that when the tube arrangement was changed from inline to staggered arrangement, the heat transfer increased from 1,996W to 2,273W. This was primarily due to the staggered arrangement incorporating a larger frontal area of heat pipes than the inline arrangement.

98

99

100

101

102

103

Further to the study carried out by Aris et al., [10] on using fins to enhance heat transfer, the work also investigated the thermal performance of heat pipes arranged under staggered and inline grid structures. The analysis was based on forced convection cooling, thereby indicating the use of heat pipes to carry out the heat duty. The findings indicated that a staggered arrangement of three-dimensional wings as extended surfaces with an aspect ratio of four and an angle of attack of 14° gave the highest enhancement in heat transfer in comparison to the inline arrangement.

104

105

106

107

Shabgard and Faghri [11] developed a steady-state analytical model for cylindrical heat pipes subjected to a constant heating flux. The proposed model coupled two-dimensional heat conduction in the heat pipe's surface wall along with the liquid flow in the wick and the vapour hydrodynamics. Constant fluid thermophysical properties along with axisymmetric heating and cooling were assumed

108 in the model. The heat pipe was constructed out of copper and distilled water was used as the internal
109 working fluid. The results of the analytical model were compared to full numerical simulations
110 previously conducted by the authors and good correlation was observed. The work found that in
111 certain cases exclusion of the axial heat conduction in the surface wall can cause an error of more than
112 10% in the calculated pressure drops in heat pipes.

113 Karthikeyan and Rathnasamy [12] studied the convective heat transfer of pin-fin arrays using the
114 staggered and inline arrangement. The tests were conducted for various mass flow rates of air
115 (Reynolds number ranging from 2,000 to 25,000. The cylindrical cross-section of the pin-fin array
116 included a diameter of 10mm with an overall height of 90mm. A uniform plate heater with a power
117 capacity of 1,500W was used to provide heating temperatures and temperature recordings were
118 undertaken using thermocouples at the inlet and outlet of the evaporator section. The experimental
119 results showed that the staggered pin-fin array significantly enhanced heat transfer as a result of
120 higher turbulence and downstream pressure drop. At a Reynolds number of 4,000, the heat transfer
121 rate using staggered array was approximately

122 Chaudhry et al. [4] compared different heat pipe working fluids in terms of their Merit No. for
123 particular use in building and ventilation systems. Water, ammonia, acetone, pentane and heptane
124 were equated based on their thermophysical fluid properties and the review study revealed that water
125 incorporated the highest Merit No. in relation to other working fluids. At an operating temperature of
126 293K, the Merit No. for water was 1.78×10^{11} , which was an order higher than ammonia which
127 incorporated a Merit No. of 7.02×10^{10} . In addition, with an increasing operating temperature gradient
128 from 293K to 393K, water displayed an increase in Merit No. of 64% while other working fluids
129 displayed a reduction in Merit No. as the operating temperatures were increased. As an outcome of
130 the study's findings, water was chosen as the working fluid for the current investigation.

131 In the author's previous works [1, 22-23], the effect of the heat pipes on the performance of the wind
132 catcher was investigated, highlighting the capabilities of the system to deliver the required fresh air
133 rates and cool the ventilated space. Qualitative and quantitative wind tunnel measurements of the
134 airflow through the wind catcher were compared with the computational modelling and good
135 correlation was observed. Field testing of the wind catcher was carried out to evaluate its performance
136 under real operating conditions (see Figure 2).



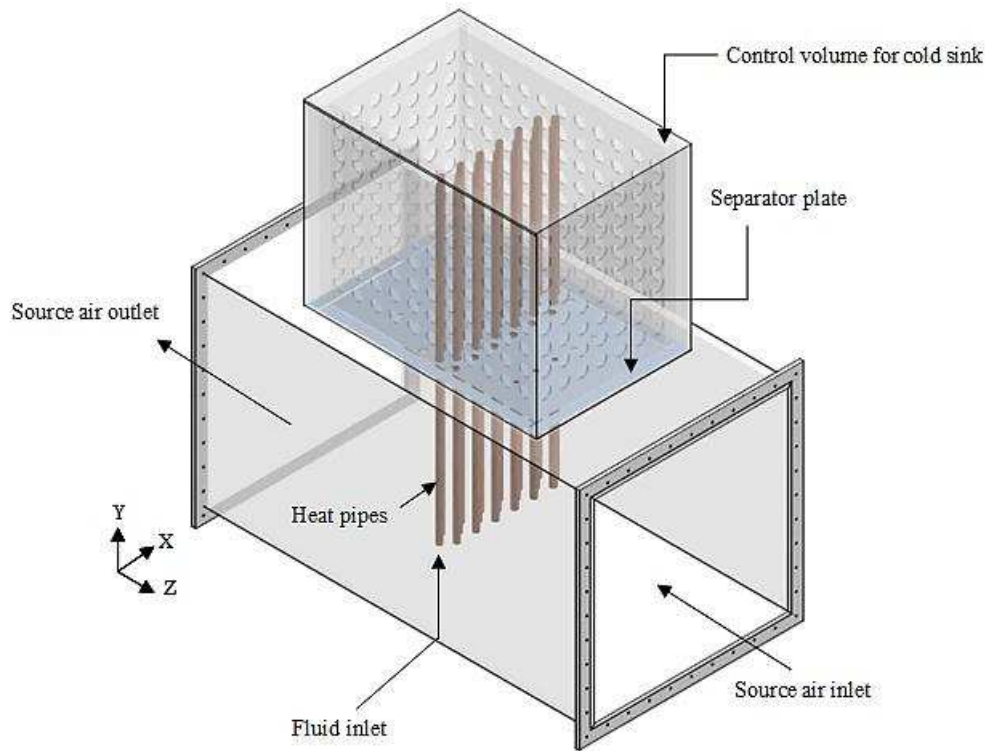
137

138 **Figure 2 Field testing of passive cooling windcatcher with heat pipe arrangements [23]**

139 This study aims to extend this work by focusing on the heat pipe arrangement optimisation. The work
140 will numerically and experimentally investigate the cooling capacity associated with heat pipes when
141 arranged in a staggered grid with streamwise distance-to-pipe diameter ratios varying between 1.0 and
142 2.0 at intervals of 0.25. Keeping the geometrical arrangement and external boundary conditions fixed,
143 the flow and thermal profiles of the subsequent airstream was analysed. The rate of heat transfer and
144 effectiveness of the system was determined using both CFD and wind tunnel testing and a correlation
145 between the results was obtained. This work will classify the optimum streamwise arrangement
146 associated with heat pipes for the purpose of passive cooling under ventilation airstreams.

147 3. COMPUTATIONAL DOMAIN

148 The computational domain comprised of the purpose-built heat pipe geometry, which was constructed
149 in order to carry out the numerical simulations alongside achieving direct experimental validation.
150 The model was designed according to the specifications of the experimental test section incorporating
151 identical dimensions. 19 cylindrical heat pipes of exact specification were used, which were oriented
152 vertically at an angle of 90° to the ground. The inner and outer diameter of the heat pipes were
153 0.015m and 0.016m. Figure 3 displays the schematic arrangement of the computational domain.



154

155 **Figure 3 Heat pipe arrangement within the computational domain**

156 The standard k-e transport model which is frequently used for incompressible flows was used to
157 define the turbulence kinetic energy and flow dissipation rate within the model [13, 14]. The use of
158 the standard k-e transport model on cylindrical pipe flows has been found in previous works [15, 16]
159 as has been the approach of integrating Eulerian-Eulerian multiphase simulations alongside [17]. The
160 turbulence kinetic energy, k , and its rate of dissipation, e , are obtained from the following transport
161 equations formulated in eqn.1 and eqn.2.

$$162 \quad \frac{\partial}{\partial t}(\rho \mathbf{k}) + \frac{\partial}{\partial x_i}(\rho \mathbf{k} u_i) = \frac{\partial}{\partial x_j} \left[\left(\mu + \frac{\mu_t}{\sigma_k} \right) \frac{\partial \mathbf{k}}{\partial x_j} \right] + \mathbf{G}_k + \mathbf{G}_b - \rho \epsilon - \mathbf{Y}_M + \mathbf{S}_k \quad (\text{eqn.1})$$

$$163 \quad \frac{\partial}{\partial t}(\rho e) + \frac{\partial}{\partial x_i}(\rho e u_i) = \frac{\partial}{\partial x_j} \left[\left(\mu + \frac{\mu_t}{\sigma_e} \right) \frac{\partial e}{\partial x_j} \right] + C_{1e} \frac{e}{k} (\mathbf{G}_k + C_{3e} \mathbf{G}_b) - C_{2e} \rho \frac{e^2}{k} + \mathbf{S}_e \quad (\text{eqn.2})$$

164 Where; \mathbf{G}_k represents the generation of turbulence kinetic energy due to the mean velocity gradients,
 165 \mathbf{G}_b represents the generation of turbulence kinetic energy due to buoyancy. \mathbf{Y}_M represents the
 166 contribution of fluctuating dilatation in compressible turbulence to the overall dissipation rate.
 167 C_{1e} , C_{2e} and C_{3e} are constants, σ_k and σ_e are the turbulent Prandtl numbers for \mathbf{k} and e . \mathbf{S}_k and \mathbf{S}_e
 168 are the user-defined source terms.

169 The Mixture multiphase model was used to solve the governing equations considering its extensive
 170 use in the study of particle transport of two-phase flows through pipes. The Mixture model solves for
 171 the mixture momentum equation and prescribes relative velocities to describe the dispersed phases.
 172 Accordingly, velocity inlet boundary conditions are applicable to both liquid and vapour phases of the
 173 fluid. The SIMPLE algorithm was used for pressure-velocity coupling in order to incorporate the mass
 174 transfer terms implicitly into the general matrix and to solve for corrections of pressure and velocity
 175 sequentially. Second Order Upwind discretisation scheme was used to obtain the face fluxes for all
 176 cells, including those near the interface.

177 Mass transfer phenomenon for phase interaction between the vapour and liquid species was carried
 178 out using the evaporation-condensation mechanism involving the fluid saturation properties. The
 179 evaporation-condensation model is a systematic model [18] with a physical basis and solves the mass
 180 transfer based on the following temperature regimes as formulated in eqn.3 and eqn.4.

$$181 \quad \text{If } T > T_{sat} \quad \dot{m}_{e \rightarrow v} = \text{coeff} \times \alpha_l \rho_l + \left(\frac{T - T_{sat}}{T_{sat}} \right) \quad (\text{eqn.3})$$

$$182 \quad \text{If } T < T_{sat} \quad \dot{m}_{e \rightarrow v} = \text{coeff} \times \alpha_v \rho_v + \left(\frac{T - T_{sat}}{T_{sat}} \right) \quad (\text{eqn.4})$$

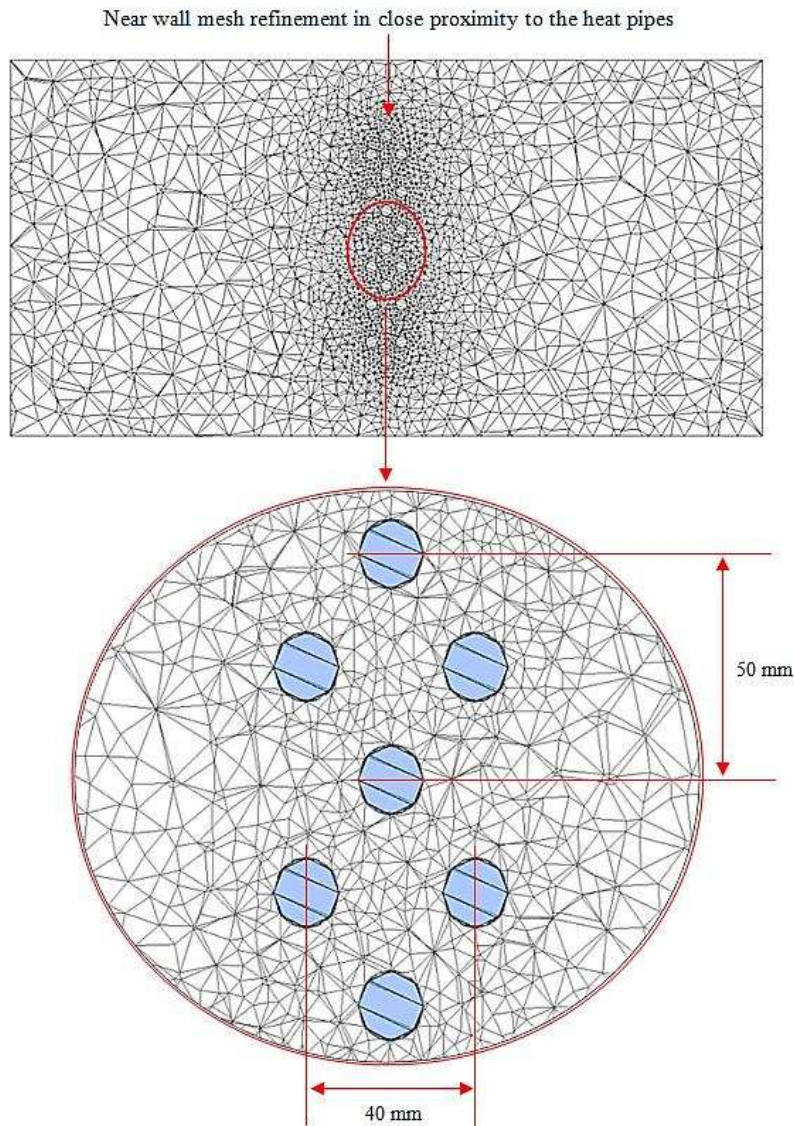
183 Where; $\dot{m}_{e \rightarrow v}$ represents the rates of mass transfer from the liquid phase to the vapour phase, α and ρ
 184 are the phase volume fraction and density.

185 3.1 Mesh generation

186 Mesh generation is one of the most important processes in CFD simulation. The quality of the mesh
 187 plays a significant role on the accuracy of results and the stability of the solution. A mesh or grid is
 188 the representation of the continuous physical surface and volume of an object through a set of discrete
 189 x, y, z coordinates.

190 The meshed model comprised of 160,736 nodes and 778,932 combined tetrahedral and hexahedral
 191 elements to obtain a balance between the run time and the resolution in the channel axial direction.
 192 The maximum and minimum sizes of the mesh elements were obtained at 7.33×10^{-2} m and 3.66×10^{-4} m
 193 while the maximum face sizing was 3.66×10^{-2} m. Higher resolution of mesh was used on the heat
 194 pipes (near wall mesh refinement) and in close proximity while lower resolution was used further
 195 away from the subject in order to obtain superior precision of results. A total of 7,799 hexahedral
 196 elements were applied on the heat pipe tubes with the grid lines perpendicular to the wall surfaces for

197 accurately resolving the viscous and thermal boundary layer. Figure 4 displays the mesh generation on
198 the computational domain.



199

200 **Figure 4 Schematic showing high resolution used in the proximity of the pipes, and lower resolution at a**
201 **larger distance away from the pipes**

202 The y^+ is a non-dimensional wall distance for a wall-bounded flow commonly used in boundary layer
203 theory and can be defined by eqn.5.

204
$$y^+ = \frac{u_* y}{\nu}$$
 (eqn.5)

205 Where u_* is the friction velocity at the nearest wall, y is the distance to the nearest wall and ν is the
206 kinematic viscosity of the fluid. The critical y^+ values of the grid on the walls of the heat pipe were in
207 the range of 28 and 45, with the average weighted average across the axial length of the heat pipe
208 tubes being 37 remained as per the recommended range which constitutes to $y^+ > 30$ in the entire
209 domain [19, 20].

210 **3.2 Boundary conditions**

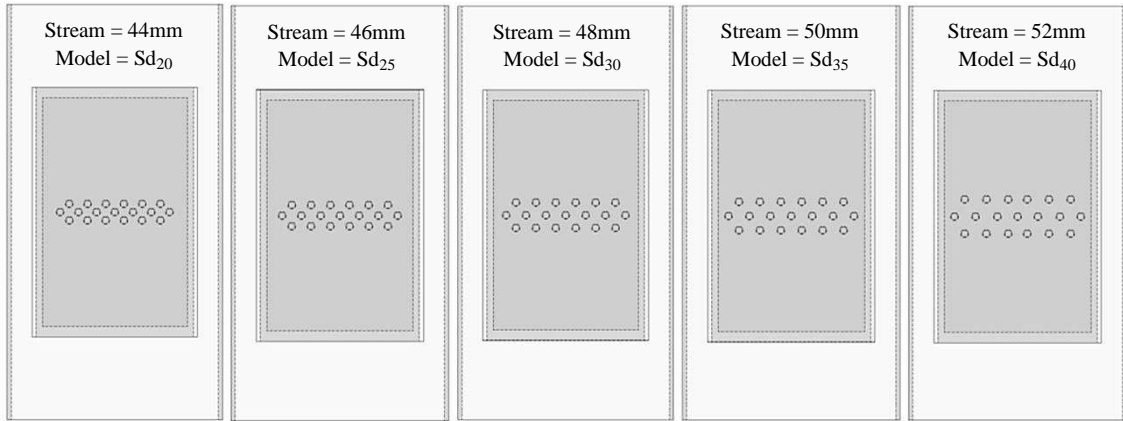
211 The applied boundary conditions on the heat pipe heat exchanger computational domain comprised of
212 an initial air velocity of 2.3m/s perpendicular to the hot channel. The cross-sectional area of the test
213 section was 0.25m² thereby indicating a Reynolds number of 62,299 (a mass flow rate of 0.631kg/sec)
214 of air at the evaporator section through convection. A source temperature of 314K was applied to the
215 evaporator section while the condenser section was maintained at 288K. Table 1 indicates the
216 summarised applied boundary conditions applied on the heat pipe heat exchanger.

217 **Table 1 Applied boundary conditions**

Parameter	Value / description
Multiphase model	Mixture model
Viscous model	k-epsilon
Near-wall treatment	Enhanced wall functions
Phase 1	Vapour
Phase 2	Liquid
Saturation temperature	293K
Inlet source temperature	314K
Inlet sink temperature	288K
Inlet air velocity	2.3m/s
Velocity formulation	Absolute
Solver type	Pressure based
Gravity	-9.81m/s ² (Y direction)

218
219 The control volume of the cold sink located directly above the evaporator section was set to a
220 temperature of 288K and was used as the condenser section of the heat pipes. The temperature in the
221 cold sink was maintained using flexible ice pockets which were positioned at all the four walls of the
222 interface. Each ice pocket had a fill volume of 12ml and a total of 49 ice pockets were used per side
223 of the cold sink. The thermal behaviour of the cold sink was initially monitored without the heat pipes
224 and the stabilised temperature was recorded for 133 minutes corresponding to 2.2 hours. This
225 information was used to determine the length of time for carrying out the experimentation involving
226 heat transfer from heat pipes.

227 Five computational models were created for the purpose of this investigation with increasing
228 streamwise arrangements between the heat pipes. The spanwise thickness (St) was kept constant at
229 50mm while the streamwise distance was increased from 20mm to 40mm in 5mm increments (Figure
230 5). In order to conduct a fair assessment, all boundary conditions were kept identical throughout the
231 thermal analyses.



232

233

Figure 5 Physical domain illustrating the streamwise distance for the analysed models

234

Table 2 indicates the ratio of increasing streamwise distances to the diameter of the heat pipe groove.

235

The ratio of Sd/D was increased from 1.0 to 2.0 while the ratio of St/D was kept fixed at 2.5.

236

Table 2 Streamwise distance models

Model	D (mm)	St (mm)	Sd (mm)	St/D	Sd/D
Sd ₂₀	20.0	50.0	20.0	2.5	1.00
Sd ₂₅	20.0	50.0	25.0	2.5	1.25
Sd ₃₀	20.0	50.0	30.0	2.5	1.50
Sd ₃₅	20.0	50.0	35.0	2.5	1.75
Sd ₄₀	20.0	50.0	40.0	2.5	2.00

237

238

4. EXPERIMENTAL SET-UP

239

The experimental testing was carried out at the University of Leeds Building Physics Laboratory

240

using a low-speed closed-loop wind tunnel to validate the numerical results. ~~The variable intensity~~

241

~~axial fan and 15kW heating elements were capable of supplying wind speeds up to 13m/s and air~~

242

~~temperatures of up to 60°C which were necessary for this study.~~ The elevation plan of the low-speed

243

closed-loop wind tunnel facility along with the experimental set-up is displayed in Figure 6. The flow

244

in the wind tunnel was characterised prior to experimental testing to indicate the non-uniformity and

245

turbulence intensity in the test-section which was 0.6% and 0.49% and according to the recommended

246

guidelines [21, 22].

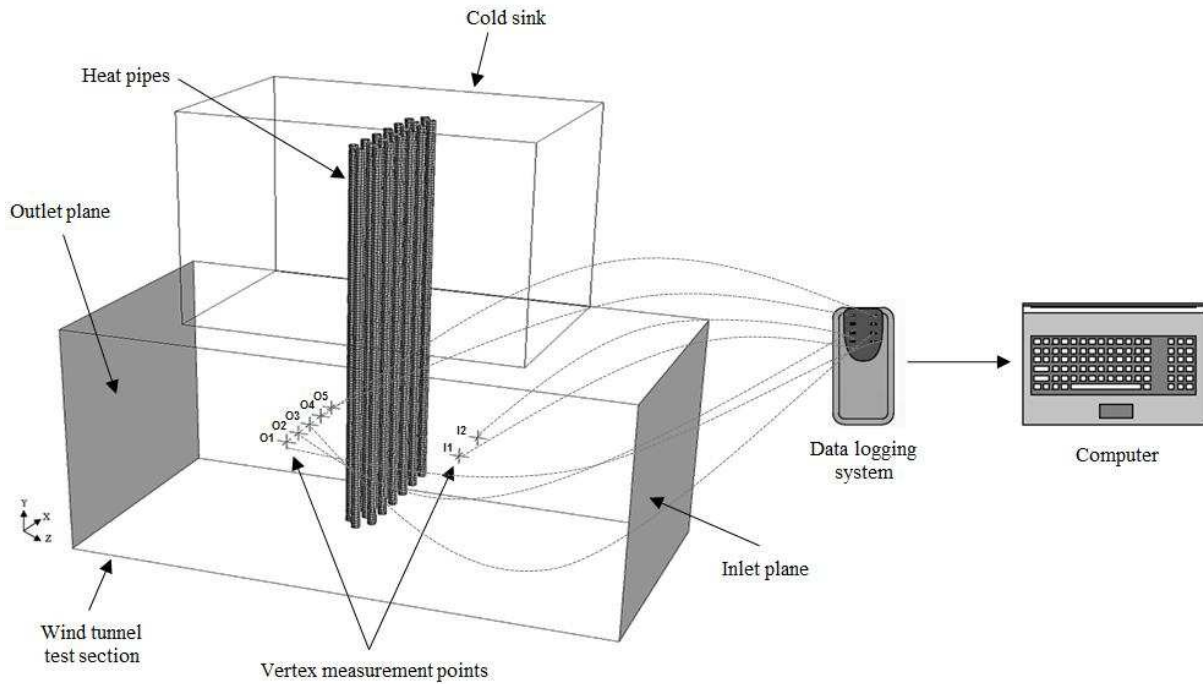


247

248 **Figure 6 Closed-loop wind tunnel showing the experimental set-up for heat pipe testing**

249 The test-section of the wind tunnel was used as the testing rig for carrying out the experimentation
 250 while the cold sink was used as the control volume for the condenser section at the top. The set-up
 251 comprised of 19 cylindrical heat pipes arranged at 90° vertical to the ground in a staggered grid with a
 252 streamwise distance of 20mm (Sd/D ratio of 1.0) and a spanwise thickness of 50mm. The diameter of
 253 the copper-water heat pipes was 16mm with a total length of 800mm. The PICO Type K
 254 Thermocouple (exposed wire, Polytetrafluoroethylene (PTFE) insulated) with a tip diameter of 1.5mm
 255 and a tip temperature range between -75°C to 250°C was used for the experiment.

256 The boundary layer thickness of the test-section was 0.05m and the heat pipes were located outside
 257 the boundary layer region for accurate evaluation. Discrete points (Figure 7) were located at the inlet
 258 and outlet of the physical domain in order to quantify the performance of the heat pipe system at
 259 specific measurement locations. The origin was the base of the test section directly underneath the
 260 central heat pipe. The thermocouple points were located 0.15m upstream (I_1 and I_2) and downstream
 261 ($O_1 - O_5$) of the heat pipe physical domain (Z-direction), spaced 0.05m apart in the X-direction. The
 262 Y-direction was kept constant at 0.25m.



263

264

Figure 7 Measurement point locations at the inlet and outlet of the physical domain

265

4.1. Heat pipe specification

266

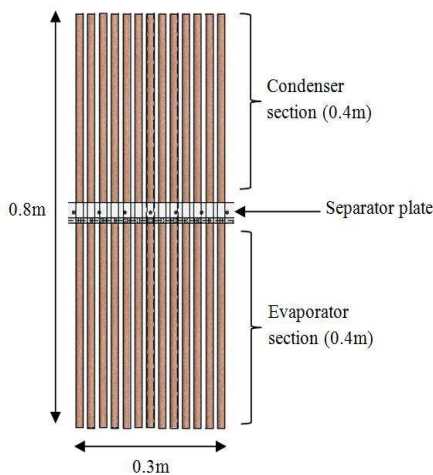
Heat pipes in the past have been integrated into the heat exchanger systems in buildings for the purpose of pre-heating fresh air. However, their potential to operate in reverse to deliver passive cooling is now gaining momentum. For this study, cylindrical copper heat pipes were manufactured as per the design specifications. The dimensions of the evaporator and condenser sections and the main parameters of the manufactured heat pipes are displayed in Figure 8.

267

268

269

270



271

272

Figure 8 Main parameters of the manufactured heat pipes

273

Description of the manufactured heat pipes	
Parameter	Value / description
Nos.	19
Pipe material	Copper
Pipe diameter	15.9 mm
Evaporator length	400 mm
Condenser length	400 mm
Total length	800 mm
Working fluid	Water / R134a
Working temperature	0-100°C
Orientation	Vertical (90°)

274 The heat pipes were charged with water and R-134a as the working fluids comprising of 2/3rd of the
 275 evaporator length, thus indicating a fluid volume of 0.000054m³. The working sub-atmospheric
 276 pressures were set to saturation and at an operating temperature of 293K. The heat pipes were vacuum
 277 sealed at the end of the tube with the end cap incorporating a diameter of 3mm greater than the actual
 278 pipe diameter. The total length of the heat pipes was 800mm and the sections were separated in the
 279 centre using a connecting plate allowing identical evaporator and condenser sectional lengths of
 280 400mm each.

281 4.2. Data reduction

282 A precise experimental determination of the thermal performance of the heat pipe heat exchanger
 283 requires accurate measurement of the temperatures of the air flow at different locations of the heat
 284 exchanger, to determine the rate of heat transfer across the length of the heat exchanger.
 285 Characterisation of the evaporator section was carried out by averaging the temperature measurements
 286 at the respective locations at regular intervals of time. Air density and specific heat capacity values
 287 were taken in accordance with the source temperatures. The rate of heat transfer at the evaporator
 288 section (test-section of the wind tunnel) is formulated using eqn.6.

$$289 \quad q_e = \rho_G U A C_{p,G} (T_{e,inlet} - T_{e,outlet}) \quad (\text{eqn.6})$$

290 Quantification of the thermal performance of heat pipes is based on the concept of heat exchanger
 291 effectiveness. The effectiveness of a heat exchanger is the ratio of actual rate of heat transfer by the
 292 heat exchanger to the maximum possible heat transfer rate between the air as formulated in eqn.7.

$$293 \quad \varepsilon = \frac{q_{actual}}{q_{max}} = \frac{T_{e,inlet} - T_{e,outlet}}{T_{e,inlet} - T_{c,inlet}} \quad (\text{eqn.7})$$

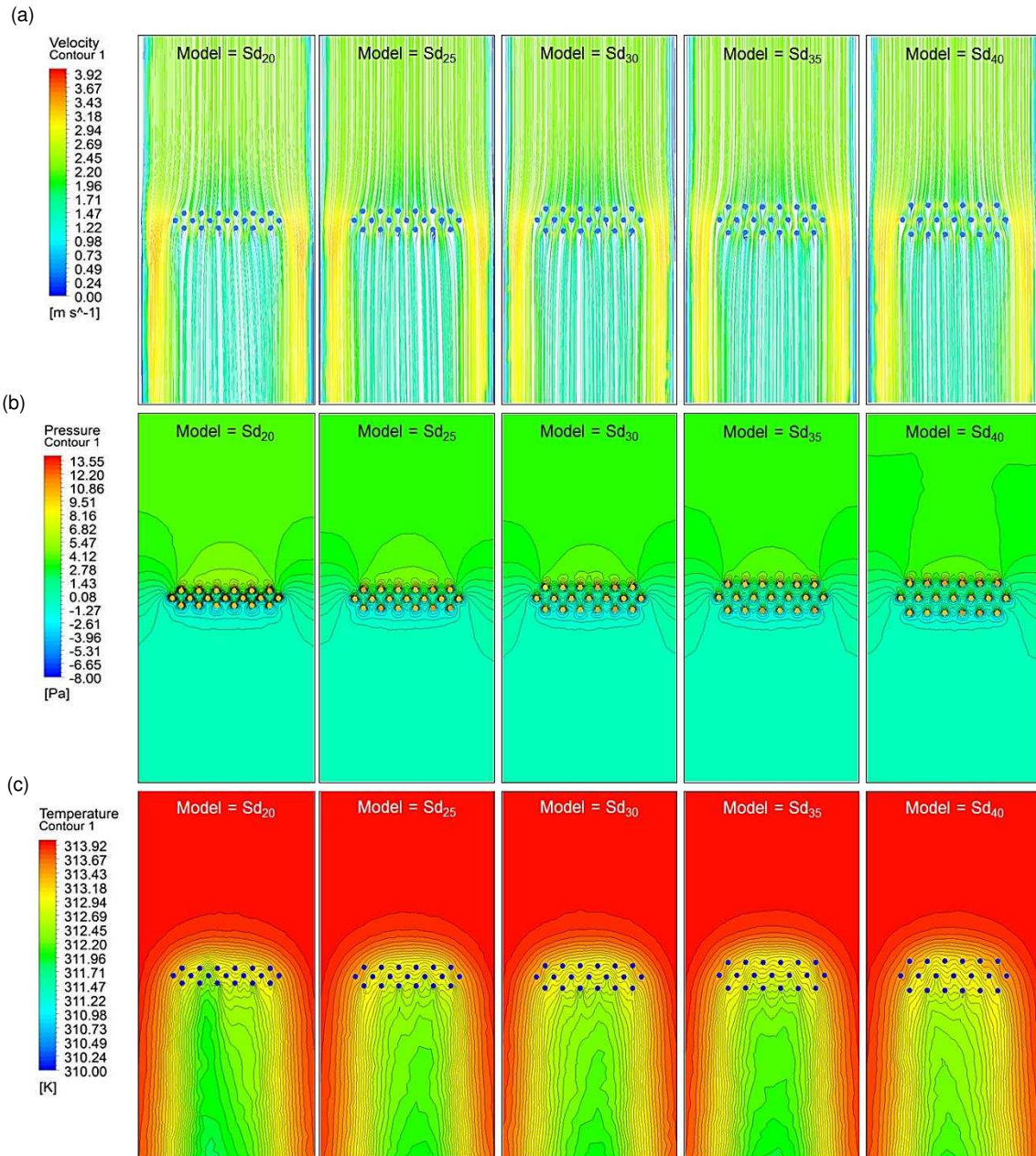
296 5. RESULTS AND DISCUSSION

297 5.1. Flow and thermal profiles

298 The computational investigation predicted the air velocity, pressure and temperature profiles upstream
 299 and downstream of the heat pipes within the test section. Based on the evaluation of the highest
 300 temperature reduction, the optimum heat pipe configuration in terms of streamwise distance was
 301 determined. **Error! Reference source not found.** Figure 9 displays the air velocity streamlines along
 302 with air pressure and temperature contour levels for each of the analysed models.

303 Figure 9 (a) displays the air velocity streamlines and due to the streamlined cross-section of the
 304 cylindrical tubes, a similar velocity trend to varying spanwise thickness models was obtained once
 305 again. The inlet velocity was kept constant at 2.3m/s for all cases and the findings showed that the
 306 velocity increased by approximately 0.9m/s at both ends of the bank of the tubes. A decrease in air
 307 velocity was noted at the immediate downstream of the heat pipes due to the contact period between
 308 the fluid and the pipe surface. With respect to Figure 9 (b), the static pressure contours for all models
 309 are highlighted. Positive pressure regions were created at the upstream of the rows of heat pipes for all
 310 analysed models with a mean value of 4.1Pa. Correspondingly, the downstream locations of the heat
 311 pipes experienced a region of negative pressures with a mean value of -0.3Pa noted across all models.

312 Temperature contour levels are illustrated in Figure 9 (c). The temperature of air decreased as the
 313 stream passed over the pipes due to the transfer of heat between the air stream and the heat pipes.
 314 Maximum temperature reduction was noted at the immediate downstream locations of the heat pipes
 315 where the air velocity was the lowest indicating a direct proportionality between the two quantities.
 316 Simultaneously, there was no temperature reduction on either side of the bank of the pipes since there
 317 was no contact between the airstream and the heat pipes.

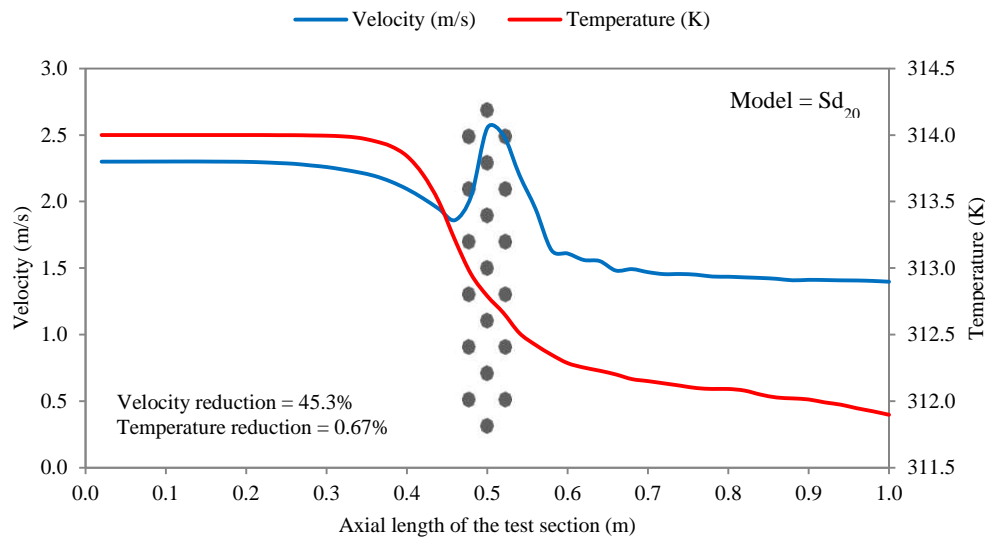


318

319 **Figure 9 Contour levels displaying air: (a) velocity (b) pressure (c) temperature for the analysed**
 320 **streamwise distance models**

321 For Sd₂₀ (streamwise distance = 20mm) model, the variation in air temperature and velocity across the
 322 axial length of the test section is displayed in Figure 10. At an inlet velocity of 2.3m/s, the maximum
 323 velocity value was determined at 2.55m/s as the airstream came in contact with the 1st row of heat

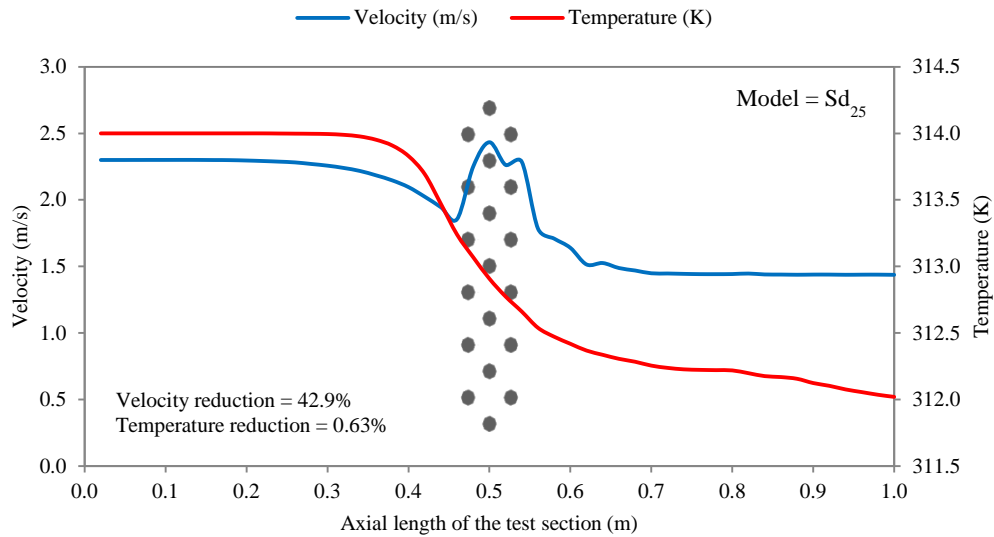
324 pipes. Overall, the air velocity was reduced by 45.3%. With respect to the airside axial thermal
 325 profile, the Sd_{20} model displayed the optimum results in terms of temperature reduction as a minimum
 326 temperature value of 311.8K was estimated, highlighting a temperature drop of 2.2K or 0.67%.



327

328 **Figure 10 Variation in air velocity and temperature profile before and after contact with heat pipes for**
 329 **Sd_{20} model**

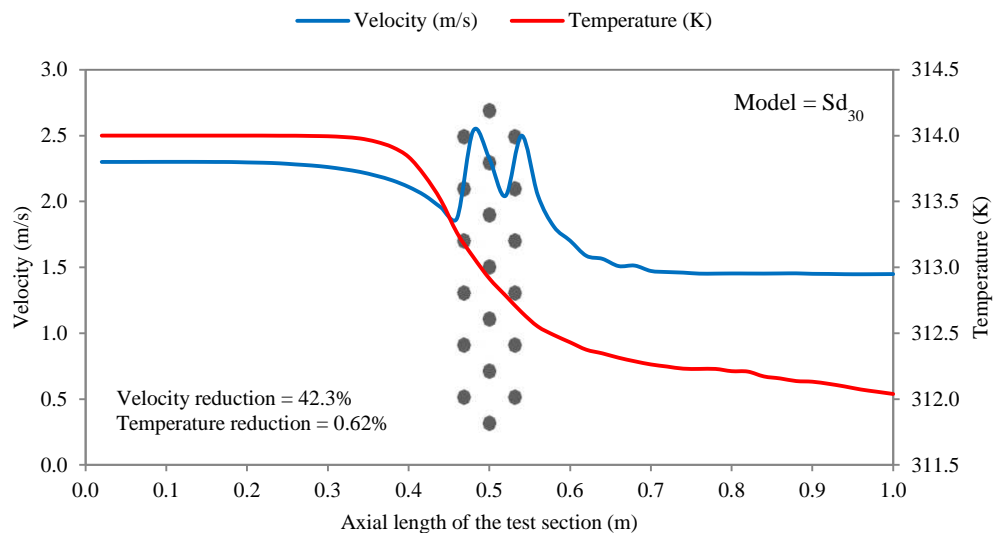
330 Figure 11 displays the quantification of air velocity and temperature results for the Sd_{25} (streamwise
 331 distance = 25mm) model. The trend in velocity profile was dissimilar to the Sd_{20} model with a
 332 maximum velocity value of 2.43m/s obtained prior to the 1st row of heat pipes. As the Sd/D
 333 (streamwise distance-to-pipe diameter) ratio increased above unit to 1.25, the formation of the second
 334 velocity peak became evident, thereby indicating a reduction in contact time between the air stream
 335 and the heat pipes. The minimum velocity value was estimated at 1.43m/s as the airstream came in
 336 contact with the three rows of heat pipes. Inlet temperature was set to 314K and a reduction
 337 percentage of 0.63% was noted for the Sd_{25} streamwise distance model in comparison to 0.67% for
 338 the Sd_{20} model.



339

340 **Figure 11 Variation in air velocity and temperature profile before and after contact with heat pipes for**
 341 **Sd₂₅ model**

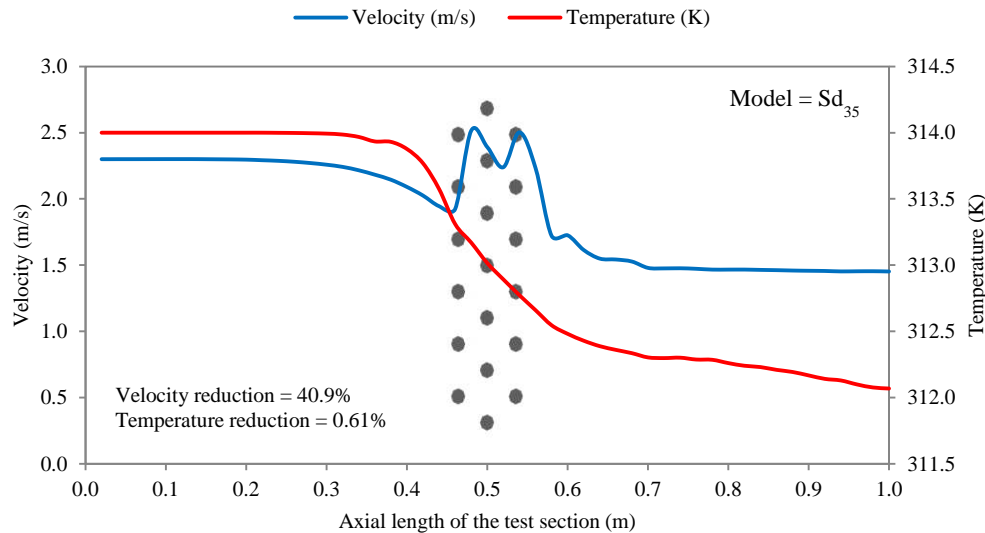
342 Figure 12 shows the air velocity and temperature trend for the Sd₃₀ (streamwise distance = 30mm)
 343 model. Like the Sd₂₅ model, two distinct velocity peak points were observed as the streamwise
 344 distance between rows was increased to 30mm. This effect was predominantly due to the increasing
 345 distances between the individual rows, providing time for the airstream to reach regions of high
 346 velocities on two instances. The maximum air velocity was determined at 2.54m/s while the mean air
 347 velocity was 1.91m/s. The temperature profile continued to indicate a lower reduction in air
 348 temperature with increasing streamwise distances as a reduction 1.96K or 0.62% was calculated.



349

350 **Figure 12 Variation in air velocity and temperature profile before and after contact with heat pipes for**
 351 **Sd₃₀ model**

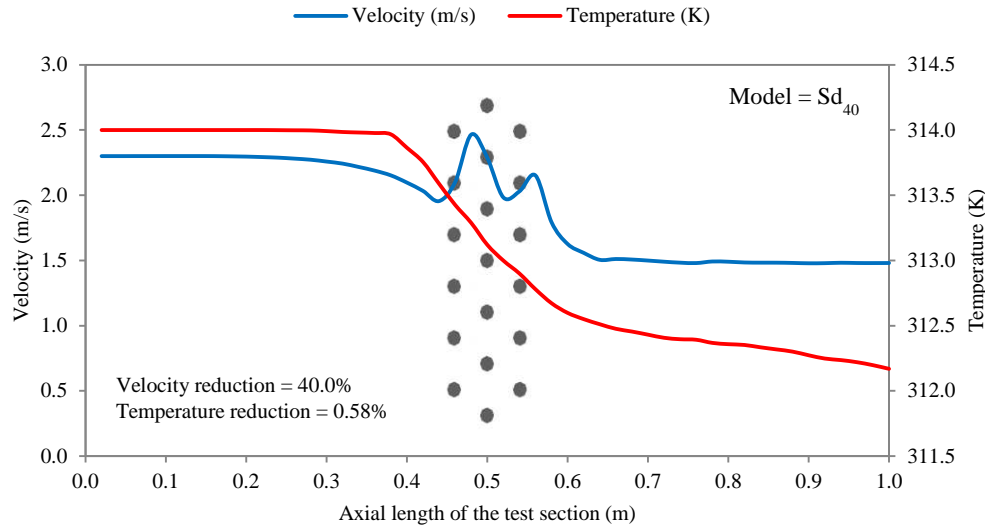
352 The streamwise distance was further increased to 35mm and the quantified air velocity and
 353 temperature results for Sd_{35} (streamwise distance = 35mm) model are displayed in Figure 13. The
 354 formation of two velocity peaks was evident at the start of the 1st and 3rd row of heat pipes. The
 355 highest velocity was noted at 2.51m/s which was 0.02m/s lower than the Sd_{30} model. The velocity was
 356 found to decrease to a minimum value of 1.45m/s downstream of the heat pipes. The air temperature
 357 decreased from the inlet value of 314K to approximately 312K after contact with the heat pipes. The
 358 temperature profile obtained from the Sd_{35} model was very similar to the Sd_{30} model as a reduction
 359 percentage of 0.61% was calculated.



360

361 **Figure 13 Variation in air velocity and temperature profile before and after contact with heat pipes for**
 362 **Sd_{35} model**

363 The maximum streamwise distance analysed from the current geometry was 40mm or twice the pipe
 364 diameter. Figure 14 displays the findings obtained from the Sd_{40} (streamwise distance = 40mm)
 365 model. A maximum velocity value of 2.46m/s was noted at the upstream of the 1st row of heat pipes.
 366 This arrangement provided the lowest reduction in air velocity as a reduction percentage of only 40%
 367 was obtained. This was due to the increased spacing between the rows of the heat pipes with the Sd/D
 368 (streamwise distance-to-pipe diameter) ratio of 2.0. With respect to the thermal profile, the Sd_{40}
 369 model indicated the lowest reduction in air temperatures, calculated at only 1.83K or 0.58%. From all
 370 analysed models it was concluded that the Sd_{20} model provided the greatest reduction in air
 371 temperatures across the axial length of the test section.



372

373 **Figure 14 Variation in air velocity and temperature profile before and after contact with heat pipes for**
374 **Sd₄₀ model**

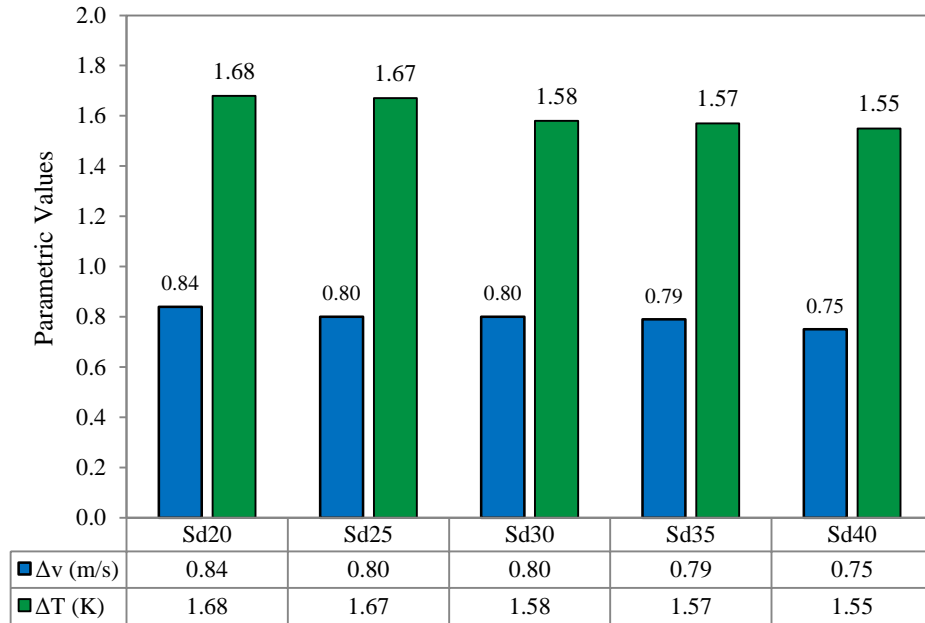
375 Table 3 summarises the mean values of the air velocity and temperature for all streamwise distance
376 models at the measurement locations. Keeping a constant inlet air temperature of 314K for all cases,
377 maximum temperature difference (ΔT) was obtained for the Sd₂₀ model at 1.68K. In general, the
378 temperature differentials decreased as the streamwise distance increased with the lowest ΔT
379 calculated for the Sd₄₀ model at 1.55K. An inverse proportionality was thus established between the
380 decreasing temperature reductions and the increasing streamwise distances between the rows of heat
381 pipes.

382 **Table 3 Summary of the mean parametric values obtained for streamwise distance models**

Model	Mean inlet velocity (m/s)	Mean outlet velocity (m/s)	Δv (m/s)	Mean inlet temperature (K)	Mean outlet temperature (K)	ΔT (K)
Sd ₂₀	2.20	1.46	0.84	313.96	312.32	1.68
Sd ₂₅	2.20	1.50	0.80	313.96	312.33	1.67
Sd ₃₀	2.19	1.50	0.80	313.97	312.42	1.58
Sd ₃₅	2.19	1.51	0.79	313.97	312.43	1.57
Sd ₄₀	2.19	1.55	0.75	313.97	312.45	1.55

383

384 In addition, the analysis determined that the mean outlet velocity increased from 1.46m/s to 1.55m/s
385 as the streamwise distance was increased from 20mm to 40mm. The maximum reduction in air
386 velocity (Δv) was calculate for the Sd₂₀ model at 0.84m/s while the minimum reduction in air velocity
387 was depicted at 0.75m/s for the Sd₄₀ model. The bar graph representation of the parametric reductions
388 in air velocity and temperature for all analysed streamwise distance models are displayed in Figure
389 15.



390

391 **Figure 15 Bar chart representation of the difference in air velocity and temperature for streamwise**
 392 **distance models**

393

394 5.2. Total cooling capacity and overall effectiveness

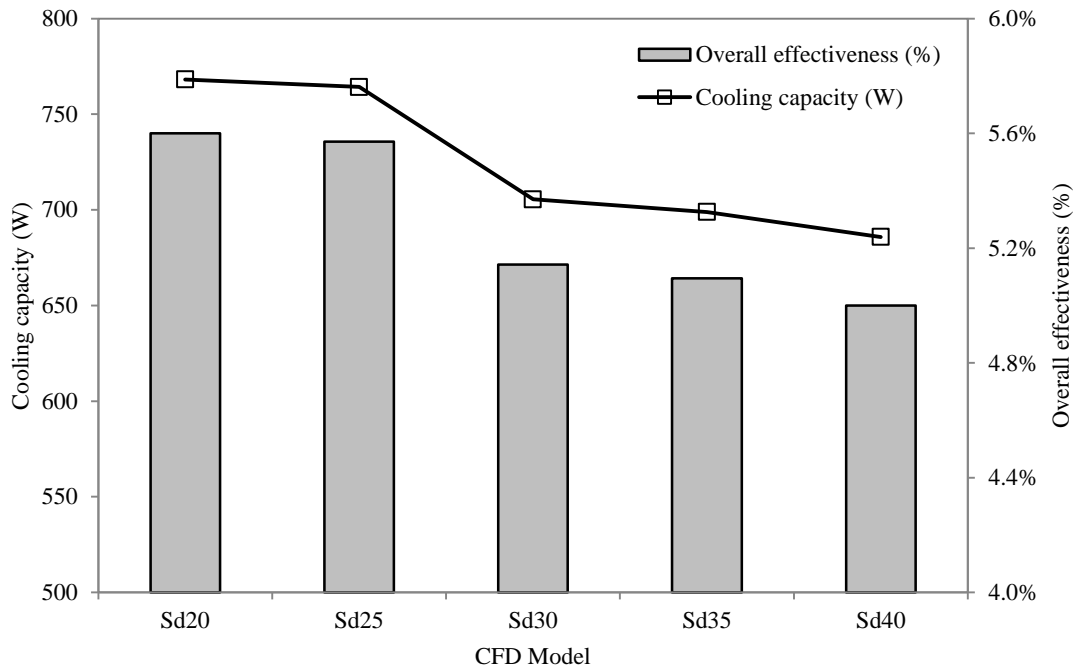
395 Similar to the spanwise arrangement models, the area-weighted averaged cooling capacity or heat
 396 transfer, upstream and downstream of the heat pipes was further evaluated. This section established
 397 the quantified results for the cooling capacity (rate of heat transfer) and effectiveness obtained from
 398 the analysis of all five streamwise distance models. The summarised findings for heat transfer and
 399 overall heat pipe effectiveness are displayed in Table 4. The highest mean overall effectiveness was
 400 calculated at 5.6% for the Sd₂₀ model while the lowest mean overall effectiveness was calculated at
 401 5.0% for the Sd₄₀ model. The highest rate of heat transfer in the test section was 768.17W for the Sd₂₀
 402 model. A variation of 82.3W was achieved between the highest and lowest rate of heat transfer from
 403 the compared models.

404 **Table 4 Summary of the mean heat transfer values obtained for streamwise distance models**

Model	Evaporator net heat transfer (W)	Overall effectiveness (%)
Sd ₂₀	768.17	5.60%
Sd ₂₅	764.25	5.57%
Sd ₃₀	705.46	5.14%
Sd ₃₅	698.93	5.10%
Sd ₄₀	685.87	5.00%

405

406 The graphical representation of the cooling capacity and heat pipe effectiveness results are plotted
 407 Figure 16. The total cooling capacity or heat transfer was directly proportional to the overall
 408 effectiveness of the heat pipe system since all other parameters apart from air temperature were kept
 409 constant throughout the investigation. Since the temperature differential reduced as the streamwise
 410 distances increased from 20mm (Model Sd₂₀) to 400mm (Model Sd₄₀), a decreasing gradient was
 411 observed for both total heat transfer rate and overall effectiveness of the heat pipe heat exchanger.



412

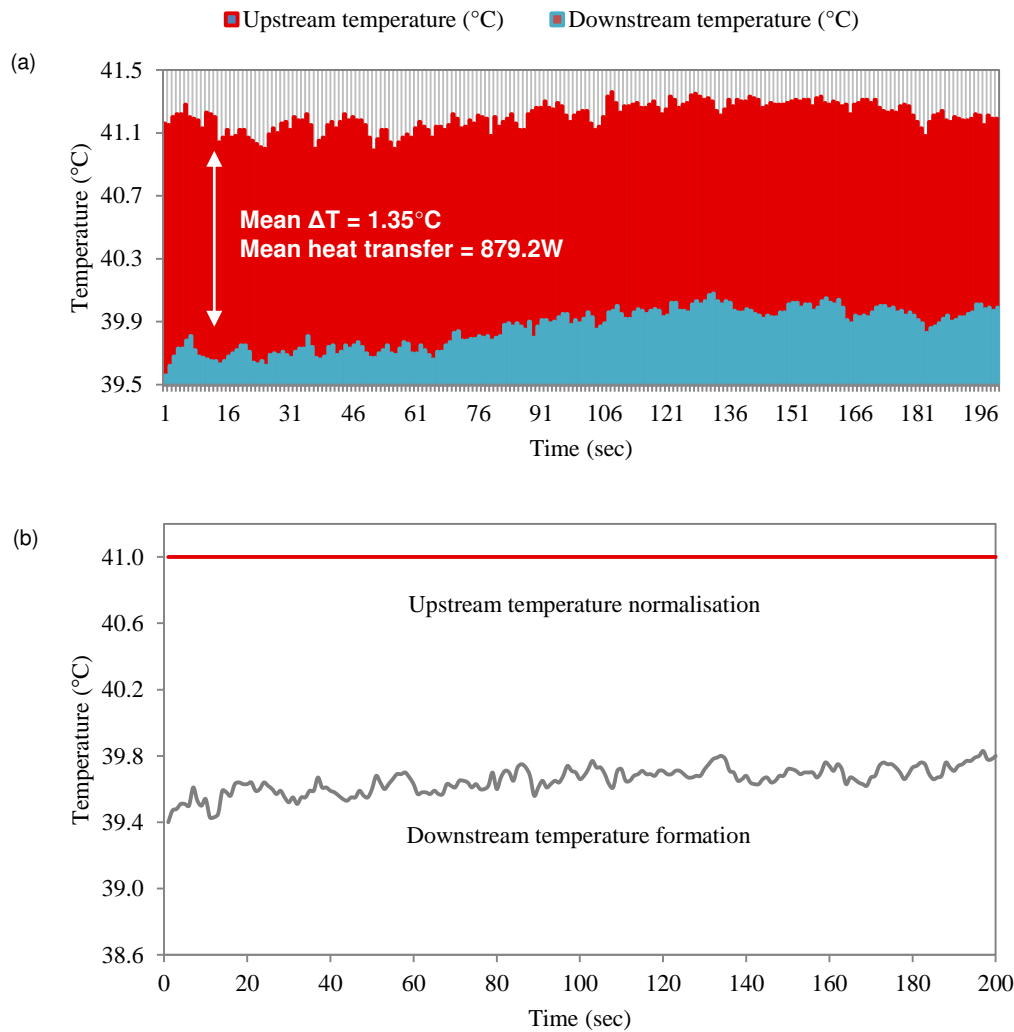
413 **Figure 16 Relationship between cooling capacity and overall heat exchanger effectiveness for streamwise**
 414 **distance models**

415 In summary, the results of this investigation indicated that the heat pipes operate at their maximum
 416 efficiency when the streamwise distance is identical to the diameter of the pipe as this formation
 417 allows the incoming airstream to achieve the maximum contact time with the surface of the pipes. The
 418 study showed that any increase in streamwise spacing leads to the formation of another bell curve
 419 representing an increase in air velocity which simultaneously reduces the contact time between the
 420 airstream and the heat pipes, decreasing its effectiveness. The findings from this study quantified that
 421 the optimum streamwise distance was 20mm at which the Sd/D (streamwise distance-to-pipe
 422 diameter) ratio was 1.0. The thermal cooling capacity was found to decrease by 10.7% from 768W to
 423 686W when the streamwise distance was increased to 40mm (Sd/D ratio of 2.0). These are important
 424 findings indicating the ideal arrangement for heat pipes to be arrayed, to work at their optimum
 425 capacity for the purpose of passive cooling in buildings.

426 5.3. Experimental validation

427 The experimental validation was carried out on the Sd₂₀ model to determine the accuracy of the
 428 numerical findings. The test-section of the wind tunnel was used as the control domain and the
 429 experimental test incorporated identical boundary conditions as the CFD model. The testing was
 430 conducted after allowing the temperature in the test-section to stabilise to the required set-point. At a

431 source temperature of 314K or 41°C, a mean reduction of 1.35°C (Figure 17 a) across was obtained
 432 using the experimental run-time of 200 seconds. Figure 17 (b) displays the formation of downstream
 433 temperatures when the source temperature was normalised to 41°C or 314K. The downstream
 434 temperature formations indicated the actual thermal cooling capacity of heat pipes in response to the
 435 source temperature. A highest temperature reduction of 1.6K was obtained during the transient test,
 436 indicating a cooling capacity of 1,045W and a heat pipe effectiveness of 6.15%.



437

438

439 **Figure 17 Upstream and downstream air temperatures formation shown in: (a) actual (b) normalised**
 440 **recordings**

441 A quantitative validation of the CFD results was done by recording temperature, velocity and pressure
 442 measurements at the discrete measurement point locations and comparing it against the
 443 experimentally obtained values. The error percentage at each measuring location for the Sd_{20} model is
 444 tabulated in Table 5. A good correlation was observed in temperature results were obtained for this
 445 model with a maximum differential of only 1.63%. Measurement location I_1 indicated the highest
 446 variation in air velocity and pressure readings with the CFD values overestimating the experimental
 447 results by 14.6% and 16.4%. In addition, a good agreement was obtained for air velocity between the
 448 two methodologies at the downstream locations with a mean error percentage of 6.4%.

449

450

451

452

Table 5 Error percentage between CFD and experimental results for Sd₂₀ model

Point	CFD (°C)	Exp. (°C)	Error	CFD (m/s)	Exp. (m/s)	Error	CFD (Pa)	Exp. (Pa)	Error
I ₁	40.97	40.95	0.05%	2.19	1.87	14.6%	3.11	2.60	16.4%
I ₂	40.96	40.98	0.05%	2.20	1.88	14.5%	3.09	2.70	12.6%
O ₁	39.31	39.60	0.74%	1.46	1.37	6.2%	1.38	1.50	8.0%
O ₂	39.02	39.40	0.97%	1.44	1.25	13.2%	1.39	1.30	6.9%
O ₃	39.32	39.71	0.99%	1.48	1.42	4.1%	1.50	1.60	6.3%
O ₄	39.38	40.02	1.63%	1.50	1.51	0.7%	1.41	1.20	14.9%
O ₅	39.59	40.23	1.62%	1.42	1.54	7.8%	1.25	1.30	3.8%

453

454

6. CONCLUSION

455 A detailed investigation was carried out into highlighting the optimum heat pipe streamwise spacing
 456 for passive cooling of high-temperature ventilation airstreams. The set-up comprised of 19 cylindrical
 457 copper-water heat pipes arranged in a staggered grid, 90° with respect to the ground. The cooling
 458 capacity or thermal performance of the heat pipes was analysed using varying streamwise distance to
 459 diameter ratios ranging from 1.0 to 2.0. The findings of this study determined that the optimum
 460 streamwise distance was 20mm at which the Sd/D (streamwise distance-to-pipe diameter) ratio was
 461 1.0. The cooling capacity and system effectiveness was found to decrease by 10.7% from 768W to
 462 686W when the streamwise distance was increased to 40mm (Sd/D ratio of 2.0). Wind tunnel
 463 experimental testing was conducted to validate the numerical model at designated point locations. A
 464 good agreement was obtained between the numerical and experimental findings with a maximum
 465 error of 1.6% for temperature and 14.6% for velocity parameters. The investigation successfully
 466 evaluated the performance of heat pipes under varying geometrical arrangement, when utilised for the
 467 purpose of pre-cooling convection airstreams, and which can be applied within windcatchers.

468

ACKNOWLEDGEMENT

469 The research and wind tunnel experimental support provided by the University Of Leeds and Qatar
 470 National Research Fund (NPRP09-138-2-059) is gratefully acknowledged by the author. The
 471 technology presented here is subject to an international patent application (PCT/GB2014/052263).

472

REFERENCES

- 473 1. Hughes BR, Chaudhry HN and Ghani SA, (2011). A review of sustainable cooling technologies in
 474 buildings, *Renewable and Sustainable Energy Reviews* 15, 3112-3120
- 475 2. Arango BS, Hughes BR and Chaudhry HN, (2012). Performance investigation of ground cooling for
 476 the airbus A380 in the United Arab Emirates, *Applied Thermal Engineering* 36, 87-95
- 477 3. Chaudhry HN and Hughes BR, (2011). Computational analysis of dynamic architecture, *Journal of*
 478 *Power and Energy, Proceedings of the Institution of Mechanical Engineers Part A* 225, 85-95

- 479 4. Chaudhry HN, Hughes BR and Ghani SA, (2012). A review of heat pipe systems for heat recovery and
480 renewable energy applications, *Renewable and Sustainable Energy Reviews* 16, 2249-2259
- 481 5. Van Fossen G, 1981. Heat transfer coefficients for staggered arrays of short pin fins, NASA
482 STI/Recon Technical Report No. 81
- 483 6. Metzger D, Fan C and Haley S, 1984. Effects of pin shape and array orientation on heat transfer and
484 pressure loss in pin fin arrays, *Journal of Engineering for Power* 106(1) 252-257
- 485 7. Chyu M, Hsing Y and Natarajan V, 1998. Convective heat transfer of cubic fin arrays in a narrow
486 channel, *ASME J. Turbomach* 120 362-367
- 487 8. Rallabandi AP, Liu YH and Han JC, 2011. Heat transfer in trailing edge wedge shaped pin fin
488 channels with slot ejection under high rotation numbers, *Journal of Thermal Science and Engineering*
489 *Applications*, 3 021007-1-9
- 490 9. Yodrak L, Rittidech S, Poomsa-ad N and Meena P, 2010. Waste Heat Recovery by Heat Pipe Air-
491 Preheater to Energy Thrift from the Furnace in a Hot Forging Process, *American Journal of Applied*
492 *Sciences* 7, 675-681
- 493 10. Aris MS, McGlen R, Owen I and Sutcliffe CJ, 2011. An experimental investigation into the deployment
494 of 3-D, finned wing and shape memory alloy vortex generators in a forced air convection heat pipe fin
495 stack, *Applied Thermal Engineering* 31, 2230-2240
- 496 11. Shabgard H, Faghri A, 2011. Performance characteristics of cylindrical heat pipes with multiple heat
497 sources, *Applied Thermal Engineering* 31, 3410-3419
- 498 12. Karthikeyan R, Rathnasamy R, 2011. Thermal performance of pin-fin arrays, *International Journal of*
499 *Advanced Engineering Sciences and Technologies* 10, 125-138
- 500 13. Launder BE and Spalding DB, 1972. *Lectures in mathematical models of turbulence*, Academic Press,
501 London, England
- 502 14. Chung TJ, (2002). *Computational Fluid Dynamics*, Cambridge University Press; illustrated edition
503 edition, ISBN-0521594162
- 504 15. Ekambara K, Dhotre MT, Joshi JB, (2006). CFD simulation of homogeneous reactions in turbulent
505 pipe flows-Tubular non-catalytic reactors, *Chemical Engineering Journal* 117, 23-29
- 506 16. Saber MH, Ashtiani HM, (2010). Simulation and CFD Analysis of heat pipe heat exchanger using
507 Fluent to increase of the thermal efficiency, *Proceedings of the 7th WSEAS International Conference*
508 *on Heat and Mass Transfer*, Cambridge
- 509 17. Ekambara K, Sanders RS, Nandakumar K, Masliyah JH, (2008). CFD simulation of bubbly two-phase
510 flow in horizontal pipes, *Chemical Engineering Journal* 144, 277-288
- 511 18. Lee WH, (1979). A Pressure Iteration Scheme for Two-Phase Modeling, Technical Report LA-UR 79-
512 975, Los Alamos Scientific Laboratory, Los Alamos, New Mexico
- 513 19. ANSYS Fluent User's Guide, (2011). ANSYS, Inc. Southpointe November 2011, 275 Technology
514 Drive, Canonsburg, PA 15317 Release 14.0
- 515 20. Versteeg HK and Malalasekera V, (2007). *An Introduction to Computational Fluid Dynamics: The*
516 *Finite Volume Method*, Second Edition, Pearson Education Limited 1995, 2007
- 517 21. Calautit JK, Chaudhry HN, Hughes BR and Sim, LF, (2014). A validated design methodology for a
518 closed-loop subsonic wind tunnel, *Journal of Wind Engineering and Industrial Aerodynamics* 125, 180-
519 194
- 520 22. Chaudhry HN and Hughes BR, (2014). Analysis of the thermal cooling capacity of heat pipes under a
521 low Reynolds number flow, *Applied Thermal Engineering* 71, 559-572
- 522 23. Calautit JK and Hughes BR (2016). A passive cooling wind catcher with heat pipe technology: CFD,
523 wind tunnel and field-test analysis, *Applied Energy*, 162, 15, 460-471